Shape-resonance-enhanced continuum–continuum coupling in photoionization of CO_2

M. R. F. Siggel, J. B. West, and M. A. Hayes
Daresbury Laboratory, Daresbury, Warrington, WA4 4AD, United Kingdom

A. C. Parr
National Institute for Standards and Technology, Gaithersburg, Maryland 20899

J. L. Dehmer
Argonne National Laboratory, Argonne, Illinois 60439

I. Iga
Departamento de Quimica, Universidade Federal de São Carlos, Via Washington Luiz, 13560, Brazil

(Received 9 March 1993; accepted 9 April 1993)

We have measured photoionization branching ratios and photoelectron asymmetry parameters for photoionization of CO_2 leading to the first four electronic states of CO_2^+ over the photon energy range from 20 to 50 eV. The motivation for this work was the prediction by Lucchese [J. Chem. Phys. **92**, 4203 (1990)] that the σ_u shape resonance in the $(4\sigma_g)^{-1}\,\tilde{C}\,^2\Sigma_g^+$ ionization channel would influence the photoionization dynamics in the other valence-shell continua through continuum–continuum channel interaction, with the main effect occurring in the $(3\sigma_u)^{-1}\,\tilde{B}\,^2\Sigma_u^+$ channel. Indeed, clear evidence for this phenomenon is observed in this channel, the most prominent indication being a broad, shallow minimum in the asymmetry parameter at $\sim$40 eV. Comparisons of the present results with theory and other measurements reflect good overall agreement and provide some guidance regarding the effectiveness of alternative approximations used in the theoretical calculations.

I. INTRODUCTION

Perhaps the best known examples of channel interaction in atomic and molecular physics are autoionization and predissociation (discrete states embedded in a continuum) and configuration interaction among discrete states. Less common are examples of prominent effects of interactions between the continuum parts of two or more channels. Continuum–continuum coupling combines two attributes that are not conducive to easy observation—weak interaction strength and spectral broadness. Nevertheless, two types of circumstances serve to showcase the interactions between continua. One approach is to examine very weak channels that are subject to interaction, and hence intensity borrowing, from intense channels. In atomic physics, a beautiful example of this approach is the $(5s)^{-1}$ photoionization channel of Xe.[1] In molecular physics, the study of a forbidden vibrational transition that appears only through vibronic interaction with an underlying continuum demonstrated the use of a weak channel to observe continuum–continuum coupling.[2,3] The second approach involves shape-resonance enhancement of continuum channel interaction. The first and best-characterized example of this approach is the $(2\sigma_u)^{-1}$ channel of N_2.[4–10] To a first approximation, this is a nonresonant ionization continuum. However, at a photon energy of $h\nu\sim30$ eV, this channel displays spectral behavior in its photoelectron asymmetry parameter that results from interaction with the σ_u shape resonance occurring at the same total energy, but in the $(3\sigma_g)^{-1}$ photoionization channel. Mechanistically, one can think of this phenomenon in the following way: first, the $3\sigma_g$ valence electron is excited into the quasibound shape resonance, where its escape through the molecular field is delayed by a potential barrier. During this delay, the excited electron collides with the core, causing an excitation of a $2\sigma_u$ electron into the $(3\sigma_g)^{-1}$ hole and the escape of the photoelectron with a kinetic energy characteristic of the $(2\sigma_u)^{-1}$ hole state. Thus, photoionization products observed in one channel may carry dynamical information from the excitation process in another channel if a mechanism exists to enhance the continuum–continuum coupling between the two. In this case, the enhancement was due to the existence of a quasibound shape resonance in one of the channels.

In this paper, we examine the photoionization of the four outermost valence orbitals of CO_2 for evidence of shape-resonance-enhanced continuum–continuum coupling. Carbon dioxide is a linear molecule in its ground state and has the following electron configuration:

$$KK(2\sigma_g)^2\,(3\sigma_g)^2\,(2\sigma_u)^2\,(4\sigma_g)^2\,(3\sigma_u)^2\,(1\pi_u)^4\,(1\pi_g)^4. \tag{1}$$

Ionization of the outer four orbitals produces the $\tilde{X}\,^2\Pi_g$, $\tilde{A}\,^2\Pi_u$, $\tilde{B}\,^2\Sigma_u^+$, and $\tilde{C}\,^2\Sigma_g^+$ states of the ion, with ionization potentials of 13.776, 17.312, 18.074, and 19.395 eV, respectively. Carbon dioxide is an interesting choice in the present context for several reasons. First, CO_2 has a very prominent σ_u shape resonance in the $(4\sigma_g)^{-1}\tilde{C}\,^2\Sigma_g^+$ photoionization channel at $h\nu\sim42$ eV.[11–26] There is evidence[25] that this shape resonance results from the trapping of the h-wave ($l=5$) component of the σ_u continuum wave function by a centrifugal barrier, the largest angular momentum shape resonance documented in molecular spectra. Other shape resonant features in the σ_g, δ_g, and π_u chan-

 0021-9606/93/99(3)/1556/8/$6.00 © 1993 American Institute of Physics

Downloaded 22 Aug 2006 to 129.6.168.231. Redistribution subject to AIP license or copyright, see http://jcp.aip.org/jcp/copyright.jsp

nels are predicted,[16–26] but are either weaker or their existence or location is still controversial. Second, the strong resonance produces a very pronounced dip in the photoelectron asymmetry parameter β at the resonance energy,[13–15] in good agreement with theory.[16–26] However, the partial cross section in this channel shows a broad peak at $h\nu \sim 32$ eV,[11,12,15] in persistent disagreement with theory.[26] This somewhat paradoxical finding prompts further, complementary studies of this resonance. Third, Lucchese[26] has performed *ab initio* calculations of interchannel coupling among the four valence levels of CO_2, providing a clear prediction of a strong shape-resonance-induced continuum–continuum coupling between the σ_u shape resonance in the $(4\sigma_g)^{-1}\,\tilde{C}\,^2\Sigma_g^+$ channel and the $(3\sigma_u)^{-1}\,\tilde{B}\,^2\Sigma_u^+$ channel. Verification of this prediction was the main goal of this work. We anticipate our results by noting that good agreement is observed between theory and the new experimental results for continuum–continuum coupling effects in the $(3\sigma_u)^{-1}\,\tilde{B}\,^2\Sigma_u^+$ channel. Furthermore, our results tend to favor Lucchese's three-channel calculation over his four-channel calculation, as discussed further in Sec. III, thus providing some guidance to theory in this case.

II. EXPERIMENT

The electron spectrometer system used in this study comprised two hemispherical electron analyzers, each arranged to detect electrons ejected at right angles relative to the horizontal photon beam. One analyzer was fixed in position, accepting electrons ejected horizontally, and the other was rotatable about the light beam through an angular range of a little more than 90° from a vertical orientation. The angular acceptance of each analyzer was limited by an aperture in its entrance lens to approximately $\pm 2°$. To enhance the sensitivity of the spectrometers, area detectors of the resistive-anode type were mounted at the exit plane of the hemispheres. Further details of the electron spectrometer system have been described by Parr *et al.*[27] Research grade CO_2 was introduced into the experimental chamber through a 0.25 mm capillary channel, providing an effusive source. A capillary light guide 2 mm in diameter channeled the vacuum ultraviolet (VUV) radiation from the exit slit of the optical monochromator to a point near the gas outlet, forming an interaction region viewed by both analyzers. The VUV radiation was provided by the Synchrotron Radiation Source at Daresbury Laboratory, a 2 GeV electron storage ring. Light was focused onto the entrance slit of a toroidal grating monochromator on the atomic and molecular science beamline. The toroidal grating monochromator and the beamline have been described by West and Padmore.[28]

The radiation from the exit slit of the monochromator is elliptically polarized, the major axis of the ellipse being horizontal. The degree of polarization for photon energies above 25 eV was determined by measuring the photoelectron angular distribution for He (whose photoelectron asymmetry parameter is known to have a value of 2) with the rotatable analyzer. For photon energies below 25 eV, Ar was used in the same fashion, using the argon β parameters published by Holland *et al.*[29] Any change in efficiency of the rotatable analyzer over its angular range was corrected by measuring the polarization on a normal-incidence monochromator both with a triple-reflection polarization analyzer and via the photoelectron angular distribution of He and by taking the result of the former as the basis for calibrating the latter. In practice, the difference in efficiency of the rotatable analyzer between the angles of 0° and 90° was $<5\%$. The transmission function (or detection efficiency) of each electron spectrometer was determined as a function of photoelectron energy and angle of ejection by using the known photoionization cross sections and angular distributions of the rare gases. The electron signal was corrected for the variation of incident light flux, which was measured by the incident flux monitor (the tungsten mesh in the polarization analyzer). The variation of the efficiency of this detector with photon energy was measured in a separate experiment. The angular distribution of the photoelectrons for dipole excitation of randomly oriented molecules is given by the expression

$$\frac{d\sigma}{d\Omega}=\frac{\sigma}{4\pi}\left[1+\frac{\beta}{4}(3p\cos 2\theta+1)\right], \tag{2}$$

where the photoelectron asymmetry parameter β completely characterizes the photoelectron angular distribution. In this expression, p is the polarization of the incoming light, θ is the angle between the major polarization axis and the ejected electron direction, and σ is the partial cross section for that channel.

The resolution of the optical monochromator used throughout the experiment varied between about 40 meV at 20 eV and 90–190 meV at 50 eV. Two sets of measurements were made. In one set, three kinetic energy ranges were collected at each photon energy, one containing the $\tilde{X}\,^2\Pi_g$ state, one containing the $\tilde{A}\,^2\Pi_u$ and $\tilde{B}\,^2\Sigma_u^+$ states, and the third containing the $\tilde{C}\,^2\Sigma_g^+$ state. From this set of measurements, β parameters for the $\tilde{X}\,^2\Pi_g$ and $\tilde{C}\,^2\Sigma_g^+$ states and branching ratios for the $\tilde{X}\,^2\Pi_g$, $\tilde{C}\,^2\Sigma_g^+$, and $(\tilde{A}\,^2\Pi_u+\tilde{B}\,^2\Sigma_u^+)$ states were determined. In this set of spectra, vibrational resolution was achieved for the $\tilde{X}\,^2\Pi_g$ and $\tilde{C}\,^2\Sigma_g^+$ states; however, the resolution was not sufficient to separate the overlapping $\tilde{A}\,^2\Pi_u$ and $\tilde{B}\,^2\Sigma_u^+$ states. In the second set of measurements, only the kinetic energy range containing the $\tilde{A}\,^2\Pi_u$ and $\tilde{B}\,^2\Sigma_u^+$ states was measured, and the resolution of the optical monochromator was continually monitored and adjusted to maintain vibrational resolution in the photoelectron spectra. These data were used to determine β parameters for the $\tilde{A}\,^2\Pi_u$ and $\tilde{B}\,^2\Sigma_u^+$ states and branching ratios for the $\tilde{A}\,^2\Pi_u$ state relative to the sum of the $\tilde{A}\,^2\Pi_u$ and $\tilde{B}\,^2\Sigma_u^+$ states. These partial branching ratios were then used to extract the separate branching ratios for the $\tilde{A}\,^2\Pi_u$ and $\tilde{B}\,^2\Sigma_u^+$ states from the composite $(\tilde{A}\,^2\Pi_u+\tilde{B}\,^2\Sigma_u^+)$ branching ratios.

III. RESULTS AND DISCUSSION

The present experimental results for branching ratios and asymmetry parameters β are given in Tables I and II.

Downloaded 22 Aug 2006 to 129.6.168.231. Redistribution subject to AIP license or copyright, see http://jcp.aip.org/jcp/copyright.jsp

TABLE I. Branching ratios for photoionization of CO_2 leading to the first four electronic states of CO_2^+.

$h\nu$ (eV)	$\tilde{X}\,^2\Pi_g$	$\tilde{A}\,^2\Pi_u$	$\tilde{B}\,^2\Sigma_u^+$	$\tilde{C}\,^2\Sigma_g^+$
20	0.343±0.026	0.301±0.028	0.327±0.044	0.029±0.002
21	0.313±0.023	0.301±0.027	0.346±0.044	0.039±0.003
22	0.284±0.020	0.318±0.024	0.348±0.038	0.050±0.004
23	0.288±0.019	0.329±0.022	0.323±0.031	0.060±0.004
24	0.292±0.019	0.338±0.021	0.300±0.027	0.069±0.005
25	0.309±0.019	0.339±0.020	0.270±0.023	0.082±0.006
26	0.333±0.022	0.336±0.019	0.239±0.019	0.093±0.006
27	0.346±0.023	0.332±0.019	0.218±0.017	0.104±0.007
28	0.349±0.022	0.326±0.018	0.211±0.016	0.114±0.008
29	0.348±0.023	0.330±0.018	0.199±0.015	0.124±0.008
30	0.354±0.023	0.323±0.018	0.193±0.015	0.129±0.009
31	0.356±0.023	0.315±0.018	0.197±0.015	0.133±0.009
32	0.355±0.023	0.310±0.017	0.193±0.015	0.143±0.010
33	0.359±0.023	0.292±0.017	0.202±0.016	0.146±0.010
34	0.358±0.023	0.278±0.017	0.210±0.017	0.154±0.011
35	0.363±0.023	0.265±0.016	0.218±0.018	0.154±0.011
36	0.361±0.023	0.256±0.016	0.224±0.019	0.159±0.011
37	0.365±0.023	0.250±0.015	0.225±0.019	0.160±0.011
38	0.370±0.024	0.247±0.016	0.230±0.019	0.153±0.011
39	0.384±0.029	0.240±0.016	0.230±0.020	0.146±0.011
40	0.393±0.047	0.243±0.021	0.229±0.023	0.136±0.011
41	0.407±0.049	0.250±0.021	0.222±0.023	0.121±0.010
42	0.420±0.047	0.248±0.022	0.225±0.028	0.107±0.009
43	0.428±0.051	0.250±0.021	0.225±0.022	0.096±0.008
44	0.441±0.053	0.237±0.025	0.233±0.033	0.087±0.007
45	0.450±0.054	0.237±0.025	0.232±0.034	0.081±0.009
46	0.469±0.057	0.229±0.024	0.225±0.033	0.077±0.010
47	0.475±0.058	0.233±0.024	0.217±0.032	0.074±0.009
48	0.480±0.059	0.227±0.024	0.220±0.032	0.073±0.009
49	0.479±0.058	0.227±0.023	0.219±0.031	0.074±0.009
50	0.482±0.060	0.227±0.023	0.216±0.031	0.075±0.010

TABLE II. Asymmetry parameters for photoionization of CO_2 leading to the first four electronic states of CO_2^+.

$h\nu$ (eV)	$\tilde{X}\,^2\Pi_g$	$\tilde{A}\,^2\Pi_u$	$\tilde{B}\,^2\Sigma_u^+$	$\tilde{C}\,^2\Sigma_g^+$
20	−0.219±0.045	0.373±0.031	−0.666±0.095	1.329±0.191
21	−0.143±0.045	0.657±0.037	−0.644±0.086	1.081±0.131
22	−0.010±0.046	0.870±0.044	−0.580±0.074	0.989±0.124
23	0.138±0.052	0.943±0.045	−0.484±0.058	1.060±0.116
24	0.300±0.060	0.975±0.047	−0.404±0.052	1.196±0.123
25	0.410±0.067	1.026±0.049	−0.268±0.048	1.326±0.139
26	0.520±0.080	1.107±0.052	−0.001±0.052	1.343±0.167
27	0.621±0.088	1.119±0.053	0.195±0.058	1.101±0.207
28	0.677±0.085	1.175±0.056	0.230±0.062	1.139±0.237
29	0.672±0.089	1.187±0.056	0.280±0.064	1.205±0.160
30	0.681±0.091	1.246±0.059	0.357±0.070	1.353±0.178
31	0.713±0.093	1.307±0.062	0.366±0.072	1.438±0.213
32	0.749±0.095	1.289±0.061	0.358±0.071	1.496±0.196
33	0.785±0.096	1.333±0.064	0.290±0.068	1.456±0.213
34	0.825±0.100	1.356±0.065	0.236±0.065	1.444±0.174
35	0.817±0.100	1.363±0.067	0.273±0.067	1.450±0.183
36	0.860±0.103	1.423±0.068	0.182±0.062	1.389±0.176
37	0.814±0.100	1.409±0.068	0.210±0.064	1.347±0.164
38	0.802±0.100	1.412±0.069	0.197±0.064	1.296±0.165
39	0.778±0.113	1.428±0.071	0.229±0.068	1.219±0.145
40	0.781±0.178	1.353±0.069	0.256±0.068	1.154±0.150
41	0.782±0.180	1.350±0.067	0.232±0.070	1.082±0.141
42	0.813±0.245	1.360±0.069	0.228±0.105	1.048±0.135
43	0.847±0.188	1.292±0.074	0.324±0.074	1.023±0.133
44	0.848±0.190	1.366±0.085	0.336±0.107	1.005±0.128
45	0.860±0.188	1.397±0.086	0.418±0.122	1.024±0.166
46	0.844±0.190	1.382±0.085	0.455±0.127	1.063±0.228
47	0.849±0.191	1.314±0.083	0.448±0.131	1.112±0.225
48	0.854±0.192	1.318±0.085	0.489±0.134	1.159±0.240
49	0.892±0.197	1.284±0.084	0.531±0.136	1.201±0.242
50	0.894±0.201	1.350±0.085	0.555±0.139	1.200±0.237

To facilitate comparison with theory, we have also calculated partial cross sections by multiplying our experimental branching ratios by the total cross section values of Brion and Tan.[11] These and the asymmetry parameters are shown in the figures, together with previously published data and the *ab initio* calculations by Lucchese[26] of the effects of interchannel coupling on these observables. The partial cross section data of Gustafsson *et al.*[12] contain a small angular dependence, since their branching ratios were not measured at the magic angle to ensure that they would be independent of the β parameters for alternative ionization channels. Their measured branching ratios B_m are related to the magic-angle branching ratios B_0 by $B_m = B_0(1-0.16\beta)$. Using this relation and our data for B_0 and β, we estimated that the angle dependence in their data is $<2\%$. Since this relatively modest angle dependence did not significantly affect the following discussions, we have used the uncorrected data of Gustafsson *et al.*[12]

The most relevant theoretical results were the calculations by Lucchese,[26] who performed *ab initio* calculations of interchannel coupling in a frozen-core Hartree–Fock (FCHF) basis for the four ionization channels measured in this work. As mentioned earlier, it was this calculation that stimulated these measurements. Three different levels of approximation are presented in each figure—a single-channel calculation, a three-channel coupled calculation in which the $1\pi_g \rightarrow k\pi_u$ channel was not coupled to the other three channels, and a fully coupled four-channel calculation. In the first two of these, the $1\pi_g \rightarrow k\pi_u$ channel was calculated in a triplet potential to eliminate the effects of the strong $1\pi_g \rightarrow 2\pi_u$ valence transition, which is not well represented in this approximation. Carrying out the $1\pi_g \rightarrow k\pi_u$ calculation in the singlet potential leads to an exaggerated cross section in this channel near the ionization limit. Hence, we have not included this single-channel approximation in the comparison with data (see the discussion by Lucchese[26] for more details on this point). The substantial differences that exist among the theoretical approximations in certain channels and in certain spectral ranges present the opportunity to use the new experimental results to provide some guidance as to the most realistic approximations in specific cases.

The following sections discuss the results for the four ionization channels studied in the present measurements: We discuss the $(4\sigma_g)^{-1}\,\tilde{C}\,^2\Sigma_g^+$ ionization channel first because the well-known effects of the strong σ_u shape resonance are prominently displayed in this channel. We then discuss the $(3\sigma_u)^{-1}\,\tilde{B}\,^2\Sigma_u^+$ channel for it is in this channel that Lucchese predicted and we confirm strong continuum–continuum coupling with the σ_u shape resonance. We then discuss the $(1\pi_u)^{-1}\,\tilde{A}\,^2\Pi_u$ and $(1\pi_g)^{-1}\,\tilde{X}\,^2\Pi_g$ channels, respectively, where the effects of

Downloaded 22 Aug 2006 to 129.6.168.231. Redistribution subject to AIP license or copyright, see http://jcp.aip.org/jcp/copyright.jsp

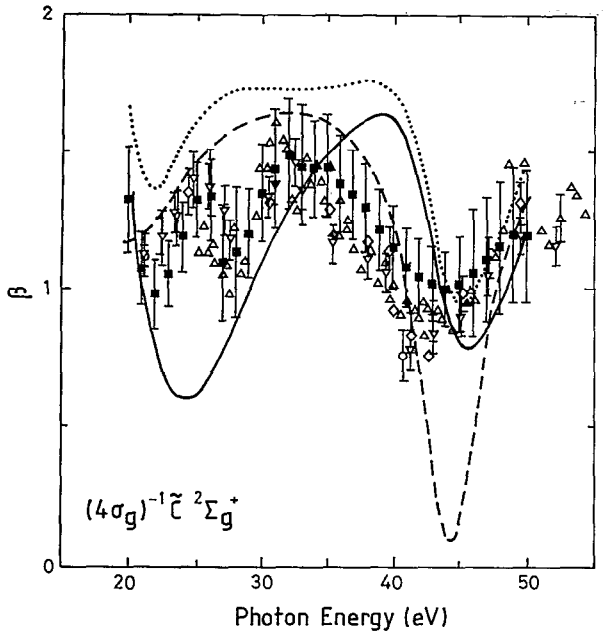

FIG. 1. Photoelectron asymmetry parameters for the $(4\sigma_g)^{-1}\,\tilde{C}\,^2\Sigma_g^+$ photoionization channel of CO_2: ■, present data; △, data of Roy *et al.* [constant-ionic-state (CIS) mode] (Ref. 15); ▽, data of Grimm *et al.* (Ref. 14); ◇, data of Roy *et al.* (full angular analysis) (Ref. 15); ○, data of Katsumata *et al.* (Ref. 30); ---, single-channel calculation of Lucchese (Ref. 26); ···, three-channel calculation of Lucchese (Ref. 26); —, four-channel calculation of Lucchese (Ref. 26).

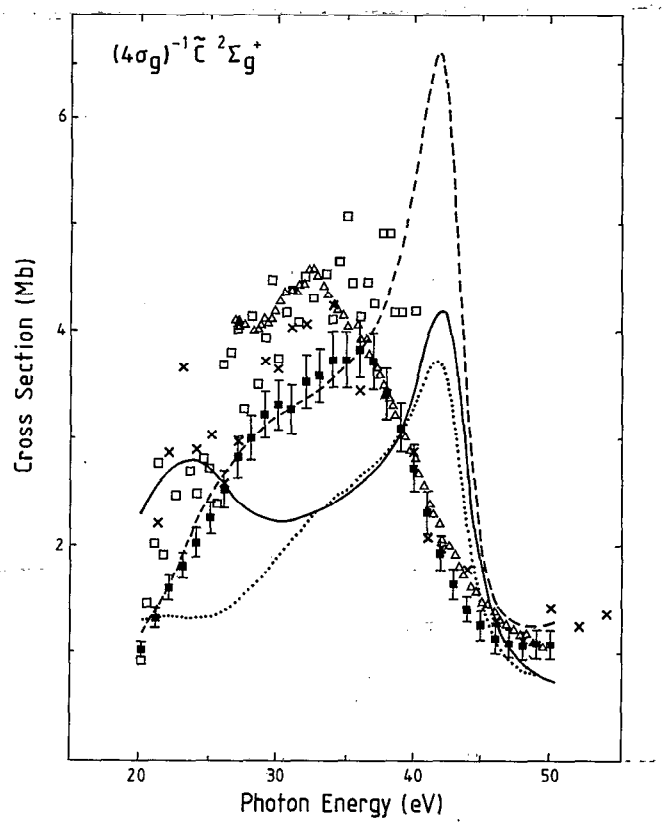

FIG. 2. Partial cross section for the $(4\sigma_g)^{-1}\,\tilde{C}\,^2\Sigma_g^+$ photoionization channel of CO_2: ■, present data; △, data of Roy *et al.* (CIS mode) (Ref. 15); ×, data of Brion and Tan (Ref. 11); □, data of Gustafsson *et al.* (Ref. 12); ---, single-channel calculation of Lucchese (Ref. 26); ···, three-channel calculation of Lucchese (Ref. 26); —, four-channel calculation of Lucchese (Ref. 26).

shape resonances and channel interaction are much less obvious.

A. $(4\sigma_g)^{-1}\,\tilde{C}\,^2\Sigma_g^+$ channel

The photoelectron asymmetry parameter and partial cross section for the oft-studied $(4\sigma_g)^{-1}\,\tilde{C}\,^2\Sigma_g^+$ ionization channel are presented in Figs. 1 and 2, respectively. The different sets of data are in overall good agreement, given the experimental uncertainties. The resulting experimental picture is of a β curve with high average asymmetry and three minima—a large, broad one at $h\nu\sim42$ eV and two less prominent features at lower photon energies. The three theory curves—one single-channel calculation and two different coupled-channel calculations—are taken from Lucchese.[26] The feature at $h\nu\sim42$ eV is caused by the shape resonance in the σ_u ionization continuum, which has been the central object of many studies.[11–26] Its presence in valence-shell spectra is thus well established, and the close connection with the corresponding resonance in electron scattering has also been discussed.[25] The comparison between experiment and the single-channel calculation reflects many earlier such comparisons, where the single-channel calculation produces a dip in β that is too deep and too narrow relative to experiment. There has been evidence[18] that averaging over vibrational motion will tend to smear out the single-channel result, but calculations of this effect at the FCHF level[22,24] have failed to reproduce the experimental shape. The coupling between ionization channels, on the other hand, is very successful in reproducing the magnitude and width of the experimental feature, although the location is still 1–2 eV too high. This feature does not clearly distinguish between the two coupled-channel calculations, although the three-channel calculation agrees slightly better with the composite data at high energy.

The minimum in β at $h\nu\sim22$ eV is more clearly established in the present data than in the earlier measurements. The origin of this feature is suggested by the theoretical curves, of which the coupled-channel curves clearly exhibit minima in this region. Continuum–continuum coupling permits the $(4\sigma_g)^{-1}\,\tilde{C}\,^2\Sigma_g^+$ ionization channel to couple to the $(3\sigma_u)^{-1}\,\tilde{B}\,^2\Sigma_u^+$ ionization channel, which exhibits a σ_g shape resonance a few electron volts above threshold. At the same photon energy, the $(3\sigma_u)^{-1}\,\tilde{B}\,^2\Sigma_u^+$ ionization channel is characterized both by a peak in the partial cross section that is much larger than that in the $(4\sigma_g)^{-1}\,\tilde{C}\,^2\Sigma_g^+$ ionization channel and also by a negative β. We conclude, as did Roy *et al.*[3] earlier, that this minimum is, at least in part, a result of the weaker $(4\sigma_g)^{-1}\,\tilde{C}\,^2\Sigma_g^+$ channel coupling to and taking up the characteristics of the stronger $(3\sigma_u)^{-1}\,\tilde{B}\,^2\Sigma_u^+$ channel by continuum–continuum coupling. Clearly, the three-channel calculation represents this interaction much better than does the four-channel calculation. This study was motivated by the search for evidence for transfer of σ_u shape resonance character from the $(4\sigma_g)^{-1}\,\tilde{C}\,^2\Sigma_g^+$ ionization channel to the $(3\sigma_u)^{-1}\,\tilde{B}\,^2\Sigma_u^+$ ionization channel, so it is most interesting to note the

Downloaded 22 Aug 2006 to 129.6.168.231. Redistribution subject to AIP license or copyright, see http://jcp.aip.org/jcp/copyright.jsp

reciprocity in the transfer of shape resonance effects between these two channels. It is also possible that the dip in β at $h\nu \sim 22$ eV may arise at the single-channel level if the shape at threshold actually constitutes part of a minimum that could move into the continuum due to intrachannel interaction. Even if this were the case, it is likely that channel interaction would contribute as well. The minimum in β at $h\nu \sim 28$ eV is less easily explained. Note that none of the theory curves displays such a feature, so that continuum–continuum coupling is not a likely cause. This dip more likely results from autoionization of multiply excited states converging either to the numerous multiply excited states of the ion that have been identified[31] in the 22–40 eV region or to the double ionization limit at 37.7 eV.[32]

The partial cross section for the $(4\sigma_g)^{-1}\,\tilde{C}\,^2\Sigma_g^+$ ionization channel is shown in Fig. 2, which clearly displays the persistent puzzle regarding the role of the σ_u shape resonance in this channel. The theory curves predict a prominent resonance at $h\nu \sim 42$ eV, with the single-channel calculation being characteristically stronger than the coupled-channel results. The data, on the other hand, show a much broader peak at significantly lower energy. The different data sets do not agree particularly well at lower energy, where the present set displays a steady decline toward threshold, in (fortuitous) agreement with the single-channel calculation and in variable degrees of agreement with earlier data. The low-energy behavior of the partial cross section in this channel does little to distinguish the relative merits of the various calculations. Moreover the persistent differences between experiment and theory in Fig. 2 remain to be satisfactorily explained. To quote Lucchese,[26] "One possible explanation of this discrepancy between theory and experiment would be that the $(4\sigma_g)^{-1}$ hole state is not well represented by a FCHF wave function, and that hole relaxation and configuration interaction must be included in the description of the ion state before accurate theoretical results can be obtained for an ion state which is 5.6 eV above the ground states of the ion." Of course, there are also the unknown effects of the interactions with the many closed channels in this energy range as well as the interactions with bent states and dissociative states.[31] No matter what the eventual explanation, however, this ionization channel in CO_2 will remain an excellent example of the importance of examining complementary observables in describing the dynamics of a process. In this case, the interference embodied in β agrees satisfactorily with current theoretical results, whereas the more straightforward dipole amplitude deviates markedly from theory, thus providing very different impressions.

B. $(3\sigma_u)^{-1}\,\tilde{B}\,^2\Sigma_u^+$ channel

The main new result from this measurement is the β and partial cross section for the $(3\sigma_u)^{-1}\,\tilde{B}\,^2\Sigma_u^+$ ionization channel presented in Figs. 3 and 4. The data in Fig. 3 clearly display energy regions in which either the single-channel or the coupled-channel behavior is apparent. At low photon energy, the data follow the deep dip in the β curve that is caused by the σ_g shape resonance located

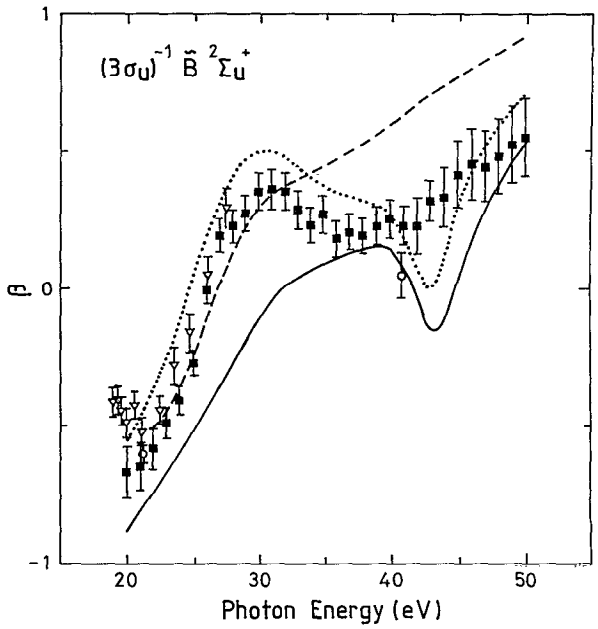

FIG. 3. Photoelectron asymmetry parameters for the $(3\sigma_u)^{-1}\,\tilde{B}\,^2\Sigma_u^+$ photoionization channel of CO_2: ■, present data; ▽, data of Grimm *et al.* (Ref. 14); ○, data of Katsumata *et al.* (Ref. 30); ---, single-channel calculation of Lucchese (Ref. 26); ···, three-channel calculation of Lucchese (Ref. 26); —, four-channel calculation of Lucchese (Ref. 26).

approximately 5 eV above threshold in this channel. At higher energies, however, the single-channel curve continues to rise toward higher energy, whereas the data and the coupled-channel curves deviate significantly from this behavior. The theoretical curves deviate from the single-channel curve starting at $h\nu \sim 30$ eV and exhibit a minimum at ~ 43 eV. This departure from the single-channel behavior is a result of coupling between the $(3\sigma_u)^{-1}\,\tilde{B}\,^2\Sigma_u^+$ ionization continuum and the σ_u shape resonance in the $(4\sigma_g)^{-1}\,\tilde{C}\,^2\Sigma_g^+$ ionization continuum. As discussed in the context of photoionization of N_2 in the Introduction, this continuum–continuum coupling is enhanced by the localized, quasibound shape resonance, which can mediate a rescattering from the resonant channel into the nonresonant channel during the delayed escape of the photoelectron. The present data clearly confirm the existence of the phenomenon as predicted by Lucchese,[26] and they are in fair agreement with the earlier high-energy data point of Katsumata *et al.*[30] The present data agree rather well with the three-channel calculation over most of the energy range; however, the dip in the calculation at $h\nu \sim 43$ eV is not present in the data.

The partial cross section for the $(3\sigma_u)^{-1}\,\tilde{B}\,^2\Sigma_u^+$ ionization channel tells a similar story, but it provides less decisive evidence for the continuum–continuum coupling than do the β data. For example, the resonant peak at low energy reflects the σ_g shape resonance. The present data and all three theoretical models agree qualitatively. However, the three-channel calculation again agrees much better with experiment throughout the low-energy range. At high energy, all three theoretical curves exhibit a secondary maximum due to increased strength in the π_g ioniza-

Downloaded 22 Aug 2006 to 129.6.168.231. Redistribution subject to AIP license or copyright, see http://jcp.aip.org/jcp/copyright.jsp

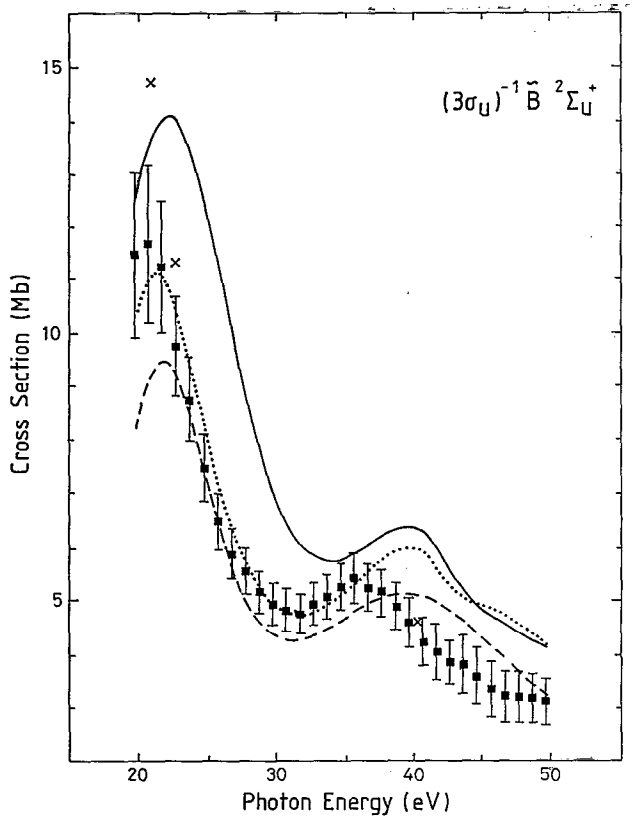

FIG. 4. Partial cross sections for the $(3\sigma_u)^{-1}\,\tilde{B}\,^2\Sigma_u^+$ photoionization channel of CO_2: ■, present data; ×, data of Brion and Tan (Ref. 11) using the branching ratios of Samson and Gardner (Ref. 33) as given in Ref. 26; ---, single-channel calculation of Lucchese (Ref. 26); ···, three-channel calculation of Lucchese (Ref. 26); —, four-channel calculation of Lucchese (Ref. 26).

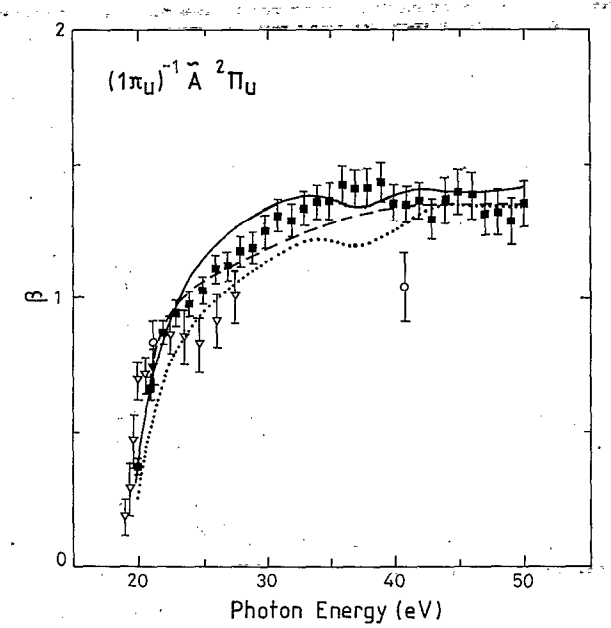

FIG. 5. Photoelectron asymmetry parameters for the $(1\pi_u)^{-1}\,\tilde{A}\,^2\Pi_u$ photoionization channel of CO_2: ■, present data; ∇, data of Grimm *et al.* (Ref. 14); ○, data of Katsumata *et al.* (Ref. 30); ---, single-channel calculation of Lucchese (Ref. 26); ···, three-channel calculation of Lucchese (Ref. 26); —, four-channel calculation of Lucchese (Ref. 26).

tion channel in this energy range; however, in addition, the coupled-channel calculations have a more articulated maximum that is due to channel interaction with the σ_u shape resonance in the $(4\sigma_g)^{-1}\,\tilde{C}\,^2\Sigma_g^+$ ionization channel. This coincidence of effects makes this observable a much less useful indicator of the presence of resonance-enhanced continuum–continuum coupling. Indeed, the data show a maximum, but it is at lower energy and does not suffice to distinguish between the theoretical models. The occurrence at lower energy is however, reminiscent of the appearance of the σ_u resonance at lower energy in the $(4\sigma_g)^{-1}\,\tilde{C}\,^2\Sigma_g^+$ ionization channel. In fact, both peaks maximize in the range 35–37 eV. This may be the only evidence in the partial cross section data, because the shape of the experimental curve is closer to that of the single-channel calculation, which does not take into account the channel interaction evident in the β results in Fig. 3.

C. $(1\pi_u)^{-1}\,\tilde{A}\,^2\Pi_u$ channel

The results in Figs. 5 and 6 for the $(1\pi_u)^{-1}\,\tilde{A}\,^2\Pi_u$ ionization channel show much smaller effects of continuum channel interaction. In Fig. 5, the present and prior data and all three theory curves show a rapid increase from $\beta\sim0$ at low energy to a flat plateau at high energy. The various data sets agree quite well, except for the high-

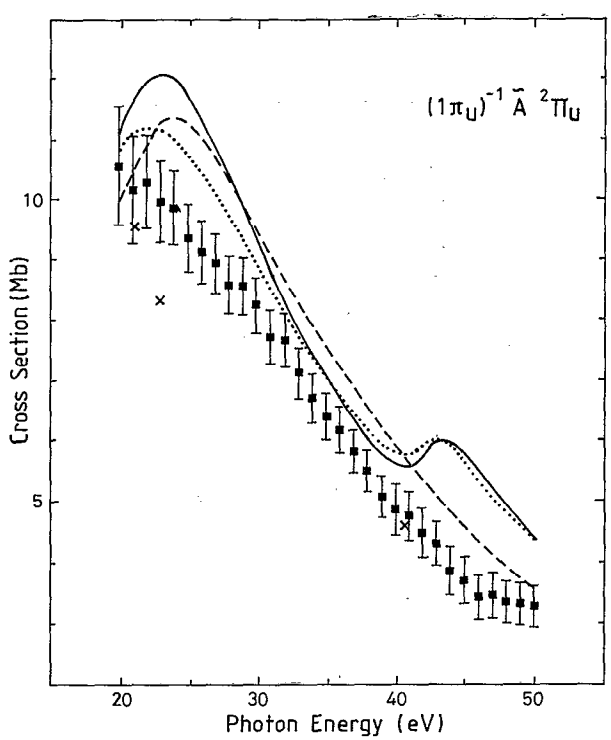

FIG. 6. Partial cross sections for the $(1\pi_u)^{-1}\,\tilde{A}\,^2\Pi_u$ photoionization channel of CO_2: ■, present data; ×, data of Brion and Tan (Ref. 11) using the branching ratios of Samson and Gardner (Ref. 33) as given in Ref. 26; ---, single-channel calculation of Lucchese (Ref. 26); ···, three-channel calculation of Lucchese (Ref. 26); —, four-channel calculation of Lucchese (Ref. 26).

Downloaded 22 Aug 2006 to 129.6.168.231. Redistribution subject to AIP license or copyright, see http://jcp.aip.org/jcp/copyright.jsp

energy point from Ref. 30. The three theory curves agree well at low energy, indicating that the method of coupling to the $1\pi_g \rightarrow k\pi_u$ channel is not important. Each coupled-channel curve contains a minor oscillation near the energy of the σ_u shape resonance in the $(4\sigma_g)^{-1}\,\tilde{C}\,^2\Sigma_g^+$ ionization channel. The data do, in fact, exhibit a faint oscillation; however, it is marginal and out of phase with the predicted oscillation. Therefore, β for the $(1\pi_u)^{-1}\,\tilde{A}\,^2\Pi_u$ ionization channel reflects good agreement between experiment and theory, but if fails to provide any clear evidence for the interchannel coupling evident in the $(3\sigma_u)^{-1}\,\tilde{B}\,^2\Sigma_u^+$ and $(4\sigma_g)^{-1}\,\tilde{C}\,^2\Sigma_g^+$ ionization channels.

The conclusion for the partial cross section of the $(1\pi_u)^{-1}\,\tilde{A}\,^2\Pi_u$ ionization channel is similar. The present data and all three theory curves in Fig. 6 show a maximum near threshold and a steady decline to higher energy. In addition, the coupled-channel curves contain a secondary maximum at $h\nu \sim 42$ eV, reflecting the coupling with the σ_u shape resonance in the $(4\sigma_g)^{-1}\,\tilde{C}\,^2\Sigma_g^+$ ionization channel. The large peak near threshold is likely to contain a contribution from the σ_g shape resonance in this channel, but it may also gain strength from the δ_g component of this ionization channel. The experimental data contain no evidence for the continuum–continuum coupling feature at 42 eV. Thus, the relatively weak signatures of this phenomenon predicted for this channel fail to appear clearly in either the β or the partial cross section curves.

D. $(1\pi_g)^{-1}\,\tilde{X}\,^2\Pi_g$ channel

The results for the $(1\pi_g)^{-1}\,\tilde{X}\,^2\Pi_g$ ionization channel are presented in Figs. 7 and 8. The present β data agree well with the earlier results reported by Grimm *et al.*[14] and by Katsumata *et al.*,[30] considering the combined error bars. All three theoretical curves also agree rather well with one another, each showing a rise starting from threshold and a decreasing slope as the excitation energy increases. The interesting point in this channel is that the $(1\pi_g)^{-1}\,\tilde{X}\,^2\Pi_g$ ionization channel contains the σ_u shape resonance, somewhere in the vicinity of $h\nu \sim 30$ eV, as well as the effects of continuum–continuum coupling to the σ_u resonance in the $(4\sigma_g)^{-1}\,\tilde{C}\,^2\Sigma_g^+$ ionization channel near $h\nu \sim 42$ eV. Indeed, both coupled-channel curves show minor features in this energy range. The two variable-wavelength data sets do show a shallow, broad minimum at $h\nu \sim 39$ eV; however, the combination of the experimental error bars and the subtlety of the predicted features prohibit us from drawing any conclusions beyond the observation that semiquantitative agreement is observed between experiment and theory. The $(1\pi_g)^{-1}\,\tilde{X}\,^2\Pi_g$ and $(1\pi_u)^{-1}\,\tilde{A}\,^2\Pi_u$ ionization channels are relatively insensitive to the σ shape resonances partly because the π and δ ionization channels are accessed from these π initial states, and this ballast tends to dilute the effects of the σ continuum.

The partial cross section for the $(1\pi_g)^{-1}\,\tilde{X}\,^2\Pi_g$ ionization channel is presented in Fig. 8. There we see that the present data are in fair agreement with the data of Gustafsson *et al.*,[12] however, the present results deviate from the data of Brion and Tan,[11] both at low energy and at higher energies. The three theoretical curves show the same general trends, but they do deviate from one another and from the data in detail, reflecting both the direct and indirect effects of the σ_u shape resonance and effects of autoionization. Unfortunately, in this case, the comparison with data does not prompt any new conclusions.

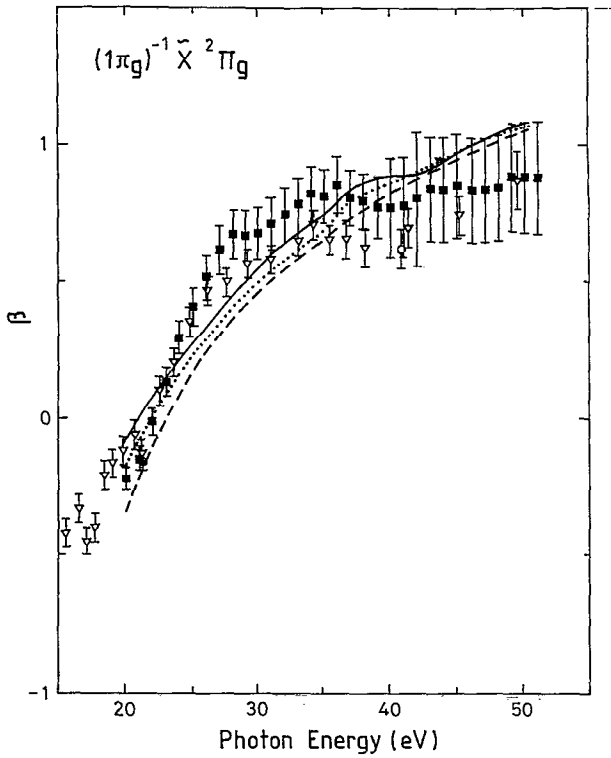

FIG. 7. Photoelectron asymmetry parameters for the $(1\pi_g)^{-1}\,\tilde{X}\,^2\Pi_g$ photoionization channel of CO_2: ■, present data; ▽, data of Grimm *et al.* (Ref. 14); ○, data of Katsumata *et al.* (Ref. 30); ---, single-channel calculation of Lucchese (Ref. 26); ···, three-channel calculation of Lucchese (Ref. 26); —, four-channel calculation of Lucchese (Ref. 26).

IV. CONCLUSIONS

We have presented the complete set of photoelectron angular distributions and partial cross sections for the four valence levels of CO_2 over the energy region $h\nu = 20$–50 eV. These data document several effects of the σ_u and σ_g shape resonances that are active in the photoionization dynamics of these channels. In particular, the present data confirm the prediction of Lucchese[26] of a large shape-resonance-induced continuum–continuum coupling effect in the $(3\sigma_u)^{-1}\,\tilde{B}\,^2\Sigma_u^+$ ionization channel. Specifically, the coupling to the σ_u shape resonance in the $(4\sigma_g)^{-1}\,\tilde{C}\,^2\Sigma_g^+$ ionization channel induces in β a significant deviation from the single-channel prediction. In fact, it is quite interesting that the $(3\sigma_u)^{-1}\,\tilde{B}\,^2\Sigma_u^+$ and $(4\sigma_g)^{-1}\,\tilde{C}\,^2\Sigma_g^+$ channels each contain a shape resonance that produces a notable feature in the β curve of the other by means of interchannel coupling in agreement with Lucchese's predictions. In general, the three-channel calculation reproduced experimental results better than did the four-channel calculation. Lucchese concluded that the failure of the four-channel results to agree with the experimental data near 20 eV and in the

Downloaded 22 Aug 2006 to 129.6.168.231. Redistribution subject to AIP license or copyright, see http://jcp.aip.org/jcp/copyright.jsp

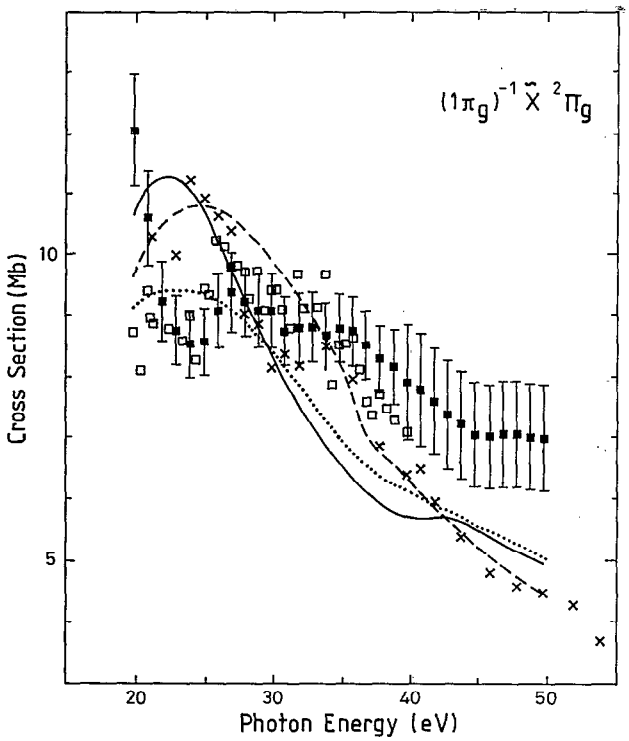

FIG. 8. Partial cross sections for the $(1\pi_g)^{-1}\,\tilde{X}\,^2\Pi_g$ photoionization channel of CO_2: ■, present data; □, data of Gustafsson *et al.* (Ref. 12); ×, data of Brion and Tan (Ref. 11); ---, single-channel calculation of Lucchese (Ref. 26); ···, three-channel calculation of Lucchese (Ref. 26); —, four-channel calculation of Lucchese (Ref. 26).

region of the σ_u shape resonance indicated the need for consideration of effects such as target correlation and polarization effects and multielectron ion states and the autoionizing states converging to them. Finally, we note that in this study, the β parameter was more useful than the partial cross section in displaying the dynamical effects of the channel interaction of interest, thus emphasizing the importance of studying complementary dynamical parameters in looking for the signature of a suspected mechanism.

ACKNOWLEDGMENTS

We would like to thank Professor Vince McKoy, California Institute of Technology, for suggesting this study. This work was supported by the U. S. Department of Energy, Office of Energy Research, Office of Health and Environmental Research, under Contract W-31-109-Eng-38; by the Science and Engineering Research Council (United Kingdom); by the Conselho Nacional de Desenvolvimento Cientifico e Tecnologico (Brazil); and by the British Council (O Conselho Britanico).

[1] J. Tulkki, Phys. Rev. Lett. **62**, 2817 (1989), and references therein.
[2] W. Domcke, Phys. Scr. **19**, 11 (1979).
[3] P. Roy, R. J. Bartlett, W. J. Trela, T. A. Ferrett, A. C. Parr, S. H. Southworth, J. E. Hardis, V. Schmidt, and J. L. Dehmer, J. Chem. Phys. **94**, 949 (1991).
[4] G. V. Marr, J. M. Morton, R. M. Holmes, and D. G. McCoy, J. Phys. B **12**, 43 (1979).
[5] S. H. Southworth, A. C. Parr, J. E. Hardis, and J. L. Dehmer, Phys. Rev. A **33**, 1020 (1986).
[6] E. D. Poliakoff, M.-H. Ho, G. E. Leroi, and M. G. White, J. Chem. Phys. **84**, 4779 (1986).
[7] J. A. Stephens and D. Dill, Phys. Rev. A **31**, 1968 (1985).
[8] B. Basden and R. R. Lucchese, Phys. Rev. A **34**, 5158 (1986).
[9] B. Basden and R. R. Lucchese, Phys. Rev. A **37**, 89 (1988).
[10] E. D. Poliakoff, S. Kakar, and R. A. Rosenberg, J. Chem. Phys. **96**, 2740 (1992).
[11] C. E. Brion and K. H. Tan, Chem. Phys. **34**, 141 (1978).
[12] T. Gustafsson, E. W. Plummer, D. E. Eastman, and W. Gudat, Phys. Rev. A **17**, 175 (1978).
[13] T. A. Carlson, M. O. Krause, F. A. Grimm, J. D. Allen, Jr., D. Mehaffy, P. R. Keller, and J. W. Taylor, Phys. Rev. A **23**, 3316 (1981).
[14] F. A. Grimm, J. D. Allen, Jr., T. A. Carlson, M. O. Krause, D. Mehaffy, P. R. Keller, and J. W. Taylor, J. Chem. Phys. **75**, 92 (1981).
[15] P. Roy, I. Nenner, M. Y. Adam, J. Delwiche, M. J. Hubin-Franskin, P. Lablanquie, and D. Roy, Chem. Phys. Lett. **109**, 607 (1984).
[16] F. A. Grimm, T. A. Carlson, W. B. Dress, P. Agron, J. O. Thomson, and J. W. Davenport, J. Chem. Phys. **72**, 3041 (1980).
[17] J. R. Swanson, D. Dill, and J. L. Dehmer, J. Phys. B **13**, L231 (1980).
[18] J. R. Swanson, D. Dill, and J. L. Dehmer, J. Phys. B **14**, L207 (1981).
[19] R. R. Lucchese and V. McKoy, J. Phys. Chem. **85**, 2166 (1981).
[20] N. Padial, G. Csanak, B. V. McKoy, and P. W. Langhoff, Phys. Rev. A **23**, 218 (1981).
[21] R. R. Lucchese and V. McKoy, Phys. Rev. A **26**, 1406 (1982).
[22] R. R. Lucchese and V. McKoy, Phys. Rev. A **26**, 1992 (1982).
[23] L. A. Collins and B. I. Schneider, Phys. Rev. A **29**, 1695 (1984).
[24] C. Yu, R. M. Pitzer, and C. W. McCurdy, J. Phys. Chem. **92**, 3116 (1988).
[25] P. M. Dittman, D. Dill, and J. L. Dehmer, Chem. Phys. **78**, 405 (1983).
[26] R. R. Lucchese, J. Chem. Phys. **92**, 4203 (1990).
[27] A. C. Parr, S. H. Southworth, J. L. Dehmer, and D. M. P. Holland, Nucl. Instrum. Methods **222**, 221 (1984).
[28] J. B. West and H. A. Padmore, in *Handbook on Synchrotron Radiation*, edited by G. V. Marr (North-Holland, Amsterdam, 1987), Vol. 2, p. 21.
[29] D. M. P. Holland, A. C. Parr, D. L. Ederer, J. L. Dehmer, and J. B. West, Nucl. Instrum. Methods **195**, 331 (1982).
[30] S. Katsumata, Y. Achiba, and K. Kimura, J. Electron. Spectrosc. **17**, 229 (1979).
[31] P. Roy, I. Nenner, P. Millie, P. Morin, and D. Roy, J. Chem. Phys. **84**, 2050 (1986).
[32] P. Millie, I. Nenner, P. Archirel, P. Lablanquie, P. Fournier, and J. H. D. Eland, J. Chem. Phys. **84**, 1259 (1986).
[33] J. A. R. Samson and J. L. Gardner, J. Geophys. Res. **78**, 3663 (1973).

Downloaded 22 Aug 2006 to 129.6.168.231. Redistribution subject to AIP license or copyright, see http://jcp.aip.org/jcp/copyright.jsp